Edge magnetoplasmons in a wide armchair graphene ribbon with a weak superlattice potential: finite frequency gaps and zero group velocity

O. G. Balev,[1] A. C. A. Ramos,[2] and H. O. Frota[1]

[1]*Departmento de Fisica, Universidade Federal do Amazonas, 69077-000, Manaus, Brazil*
[2]*Universidade Federal do Ceará, Campus Cariri, 63040-360, Juazeiro do Norte, Ceará, Brazil*

We show strong effects of a weak and smooth, on the magnetic length, superlattice potential upon edge magnetoplasmons (EMPs) at the armchair edge, with a smooth steplike electrostatic lateral confining potential, of a wide graphene channel in the $\nu = 2$ quantum Hall effect regime. The superlattice potential leads to essential enlargement of a number of EMPs, descend from two fundamental EMPs in the absence of superlattice. For the wave vector k_x within the first Brillouin zone, the EMPs show as the regions of acoustical or quasi-acoustical dispersion, with a finite value of group velocity, so the regions with frequency gaps, where a group velocity is nullified at some k_x. We obtain that for $k_x \to 0$ only for two EMPs the frequency tends to zero as for other EMPs it obtains finite values. Strong dependence of dispersion relations of the EMPs from the period of the superlattice a_0 and the distance d from a metallic gate is shown; in particular, for typical size of a gap, for characteristic value of the frequency and k_x at which the group velocity is reduced to zero. At the frequency that corresponds to zero group velocity of pertinent fundamental EMP branch the response of the system should present a strong resonance.

I. INTRODUCTION

Graphene after experimental discovery of its high-quality freestanding samples,[1] has attracted a strong attention.[2] Charge carriers in a single-layer graphene possess a gapless, linear spectrum close to the K and K' points[1–3] and manifest behavior of chiral massless particles with a "light speed" equal to the Fermi velocity, v_F. Graphene shows a lot of unusual effects, e.g.: the Klein paradox[2,4,5], i.e., the perfect transmission through arbitrarily high and wide barriers upon normal incidence (as far as a Dirac-type Hamiltonian is valid), a half-integer quantum Hall effect (QHE)[2,6–8], and a zitterbewegung,[2,9,10] i.e., effect induced by a lateral confinement of Dirac fermions. Properties of the latter effect are essentially modified by a strong magnetic field. Extra Dirac points in the energy spectrum for superlattices in graphene have been obtained if the amplitude of periodic potential is sufficiently large while its period is small enough.[11–13] In particular, this leads to new properties of the QHE.[11]

Graphene's edges have also been studied considerably,[2,6–8,14,15] in particular, in connection with the QHE[2,6–8]; for some phenomena it matters a type, the armchair or zigzag, of edges.[2,6–8] Edge magnetoplasmons (EMPs) in graphene have been studied only recently;[16] it is shown that in the $\nu = 2$ QHE regime at the armchair edge, and in the presence of a smooth steplike electrostatic lateral confining potential, the chirality, spectrum, spatial structure, and number of the fundamental EMPs depend strongly on the position of the Fermi level E_F.

In the case (i) of Ref. 16, when E_F intesects (see Fig. 1, cf. with Fig. 1(a) of Ref. 16) four degenerate states of the zero LL at one location and two degenerate states of this LL at a different location, two fundamental EMPs are present: counterpropagating and with essential spatial overlap. This is in contrast with EMPs in conventional two-dimensional electron systems (2DES) which give only one fundamental EMP at the $\nu = 2$ QHE regime, with negligible spin-splitting; for conventional 2DES different types of EMPs have been studied theoretically[17–23] and experimentally.[24–26] Above two counterpropagating EMPs can be on resonance if a strong coupling of the EMPs holds at the ends of the segment $L_x^{em} \leq L_x$, where L_x is the length of graphene channel.[16]

In present study for the case qualitatively outlined in Fig. 1 (i.e., it is the case (i) of Ref. 16) we explore theoretically effect of a weak and smooth superlattice potential $V_s(x) = V_s \cos(Gx)$ with $G = 2\pi/a_0$, upon EMPs. Here, in agreement with speculations of[16] that a strong Bragg coupling is possible due to a weak superlattice along the edge (with period L_x^{em}, if $L_x/L_x^{em} \gg 1$), we show that $V_s(x)$ can have a strong effect on two fundamental EMPs leading to manifestation of resonance effects; in particular, referred to in the abstract. Present EMPs in graphene with the superlattice are very different from the EMPs treated previously for conventional 2DES with a superlattice.[27]

In Sec. II A we obtain the wave functions and the spectra of LLs in an infinitely large graphene flake in the presence of a perpendicular magnetic field and of a smooth electrostatic confining potential, along the y direction, as without $V_s(x)$ so in its presence. In Sec. II B we study the combined effect of a smooth, step-like electrostatic confining potential and of armchair graphene edges, at $y = \pm L_y/2$, and of the superlattice potential $V_s(x)$ on the local Hall conductivity in the $\nu = 2$ QHE regime. In Sec. III we obtain strong renormalization of the EMPs in graphene by a weak superlattice potential. We make concluding remarks in Sec. IV.
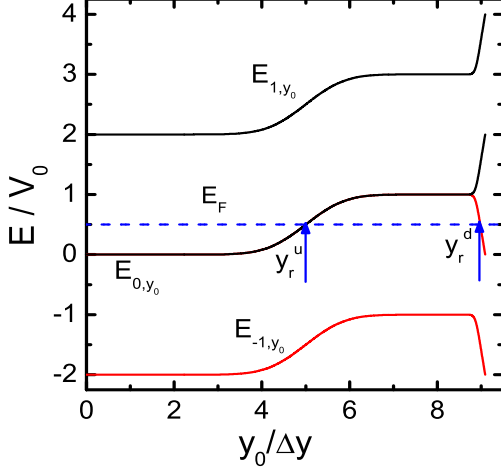
Figure 1: (Color online) Energy spectrum of the $n = 0, \pm 1$ LLs as a function of the quantum number y_0, at the right half of symmetric graphene channel with armchair edges and the smooth electrostatic potential, Eq. (9), for the Fermi level $E_F = V_0/2$. Spatially separated edge states are created at y_r^u and at y_r^d (marked by an upward arrow) as the branches of the $n = 0$ LL cross E_F. The $\nu = 2$ QHE is manifested in dc magnetotransport.

II. GRAPHENE CHANNEL AND LOCAL HALL CONDUCTIVITY

A. Effect of a smooth potential and of a weak periodic potential on the LLs

We consider a long and a wide flat graphene flake of length L_x and width L_y, with armchair edges at $y = \pm L_y/2$ in the presence of a perpendicular magnetic field $\mathbf{B} = B\hat{z}$, of a smooth confining potential $V_y = V(y)$ along the y direction of electrostatic origin, and of a one-dimensional (1D) periodic potential $V_s(x)$ along the x direction. We assume that $V_s(x) = V_s \cos(Gx)$ is a weak 1D modulation potential of period a_0. For definiteness we assume that the potential V_y is symmetric.

If it is not otherwise stated, we consider solutions with energy and wave vector close to the K point; we present pertinent results for the energies and wave vectors close to the K$'$ point (valley) as well. In the nearest-neighbor, tight-binding model the one-electron Dirac Hamiltonian, for massless electrons, is $\mathcal{H} = \mathcal{H}_0 + \mathbb{1}V_s(x)$ where $\mathcal{H}_0 = v_F\vec{\sigma} \cdot \hat{\vec{p}} + \mathbb{1}V_y$, with $\mathbb{1}$ the 2×2 unit matrix. Explicitly $\mathcal{H}_0$ is given by ($e > 0$)

$$\mathcal{H}_0 = v_F \begin{pmatrix} V_y/v_F & p_x - ip_y - eBy \\ p_x + ip_y - eBy & V_y/v_F \end{pmatrix}, \quad (1)$$

where p_x and p_y are components of the momentum operator $\mathbf{p}$ and $v_F \approx 10^6 m/s$ the Fermi velocity. The vector potential is taken in the Landau gauge, $\mathbf{A} = (-By, 0, 0)$.

1. Landau levels for a smooth potential $V(y)$

First, we present properties of the LLs in the absence of periodic potential, when only a smooth potential and armchair termination are assumed[16]. The equation $(\mathcal{H}_0 - E)\psi = 0$ admits solutions of the form

$$\psi^{(0)}(\mathbf{r}) = e^{ik_{x\alpha}x}\Phi(y)/\sqrt{L_x}, \quad \Phi(y) = \begin{pmatrix} A\Phi_A(y) \\ B\Phi_B(y) \end{pmatrix}, \quad (2)$$

where the components $\Phi_A(y)$ and $\Phi_B(y)$ correspond to the two sublattices and the coefficients A and B satisfy the relation $|A|^2 + |B|^2 = 1$; $\mathbf{r} = \{x, y\}$. Introducing the magnetic length $\ell_0 = (\hbar/eB)^{1/2}$, $y_0 = \ell_0^2 k_{x\alpha}$, the variable $\xi = (y - y_0)/\ell_0$, and assuming that V_y is a smooth function of y, with a characteristic scale $\Delta y \gg \ell_0$, it follows[16] at $r = \ell_0 a/\hbar v_F \ll 1$ for the $n = 0$ LL that the energy $E_{0,k_{x\alpha}}^{(0)} = V(y_0)$ and

$$\Phi_{A\kappa}^0(\xi) = \Phi_{B\kappa}^0(\xi) = 1/(\pi\ell_0^2)^{1/4}e^{-\xi^2/2},$$
$$A_\kappa^0 = (1/r)[1 - \kappa(1 - r^2)^{1/2}]B_\kappa^0, \quad (3)$$

where $a = \partial V/\partial \xi|_{\xi=0}$, and $\kappa = +(-)$ corresponds to the K (K$'$) valley. here $B_+^0 = A_-^0 \approx 1$ and $A_+^0 = B_-^0 \approx r/2 \ll 1$.

Finally, without periodic potential for any $n = 0, \pm 1, \pm 2, \dots$ LL and y_0 not too close to the graphene lattice termination at $y = \pm L_y/2$ (see Fig. 1), the eigenvalues $E_{n,k_{x\alpha}}^{(0),\kappa} = E_{n,y_0}^{(0),\kappa}$ can be written as

$$E_{n,k_{x\alpha}}^{(0),\kappa} = sgn(n)\frac{\hbar v_F}{\ell_0}\sqrt{2|n|} + V(y_0), \quad n = 0, \pm 1, \dots \ (4)$$

where the sign function $sgn(n) = 1$ and -1 for $n > 0$ and $n < 0$, respectively. Notice that each $n \neq 0$ LL is twice degenerate with respect to the valley quantum number κ. However, the latter index is kept in the left hand side of Eq. (4) as for $y_0(k_{x\alpha})$ close to the armchair edge these eigenvalues, and especially strongly $E_{0,k_{x\alpha}}^{(0),\kappa}$, become dependent on κ; notice, for these conditions κ can not be related only to one valley[6–8]. Accordingly, for $n \neq 0$ LL and y_0 not too close to the graphene lattice termination, see Fig. 1, the eigenvalues (4) are four times degenerate. Wave functions pertinent to the eigenvalues Eq. (4) we will denote also as $\psi_{n,k_{x\alpha}}^{(0),\kappa}(\mathbf{r})$.

2. Effect of potential $V(y)$ and of a weak smooth periodic potential $V_s(x)$ on the LLs

Assuming $\hbar v_F/\ell_0 \gg \hbar v_g(k_{x\alpha})G \gg V_s/2$ and $G\ell_0 \ll 1$ where the group velocity $v_g(k_{x\alpha}) = \hbar^{-1}dE_{0,k_{x\alpha}}^{(0)}/dk_{x\alpha}$, now we will study how a weak periodic potential $V_s(x)$ modifies energies and wave functions of the LLs for a smooth potential $V(y)$; in particular, for conditions pertinent to Fig. 1. We calculate the eigenvalues and eigenfunctions corresponding to the Hamiltonian $\mathcal{H} =$

$\mathcal{H}_0 + \mathbb{1}V_s(x)$ using the perturbation theory[28]. Because further there will be important only the eigenstates localized, along y, near a right edge of the channel, we will write formulas assuming, in particular, such eigenstates. Similar with Ref.[27], we can neglect by a small "nonresonance" contributions, $n_\beta \neq n_\alpha$. Then keeping only the "resonance" contributions, $n_\beta = n_\alpha$, and the terms of the first order over V_s, e.g., for the eigenfunctions of the $n = 0$ LL we obtain

$$\psi_{0,k_{x\alpha}}^\kappa(\mathbf{r}) = \psi_{0,k_{x\alpha}}^{(0),\kappa} + \frac{V_s}{2\hbar v_g(k_{x\alpha})\,G}\left[\psi_{0,k_{x\alpha}-G}^{(0),\kappa} - \psi_{0,k_{x\alpha}+G}^{(0),\kappa}\right]. \tag{5}$$

Further, the eigenvalues are well approximated by the zero-order terms, i.e., $E_{n,k_{x\alpha}}^\kappa \approx E_{n,k_{x\alpha}}^{(0),\kappa}$, where, for y_0 not too close to the graphene lattice termination, $E_{n,k_{x\alpha}}^{(0),\kappa}$ are given by Eq. (4). Indeed, the first order corrections are exactly nullified and the second order ones are very small, e.g.: $\sim (V_s/2V_0)^2 \ll 1$ for the model potential Eq. (9).

B. Local Hall conductivity in the $\nu = 2$ QHE regime

Extending magnetotransport formulas for the local Hall conductivity $\sigma_{yx}(\mathbf{r})$ of a standard 2DES in the channel, in the presence of a smooth lateral potential[29–31], we obtain, for linear responses and in strong magnetic fields, $\sigma_{yx}(\mathbf{r})$ in the form[32]

$$\sigma_{yx}(\mathbf{r}) = n(\mathbf{r})e/B, \tag{6}$$

where the local electron density $n(\mathbf{r})$ is smooth, on the characteristic scale ℓ_0, as along y, mainly monotonic, so along x, with a weak periodic modulation. It is given by

$$n(\mathbf{r}) = \sum_{\alpha\kappa} f_{\alpha\kappa}\langle\alpha\kappa|\mathbb{1}\delta(\mathbf{r}-\hat{\mathbf{r}})|\alpha\kappa\rangle, \tag{7}$$

with $\alpha = \{n, k_{x\alpha}\}$; $\sigma_{yx}(y) = -\sigma_{xy}(y)$. So far in Eqs. (6)-(7) only the electrons from the conduction band LLs are assumed. However, if the valence band LLs can essentially contribute to $\sigma_{yx}(\mathbf{r})$, as for Fig. 1, the local hole density $p(\mathbf{r})$ will contribute to the right hand part of Eq. (6) by changing $n(\mathbf{r})$ on $[n(\mathbf{r}) - p(\mathbf{r})]$. Then, for conditions relevant to Fig. 1, when only $(n = 0, \kappa = \pm)$ LLs can essentially contribute to $\sigma_{yx}(\mathbf{r})$ or a diagonal component of the local conductivity tensor, equation (6) is rewritten as

$$\sigma_{yx}(x,y) = \frac{2e^2 L_x}{h}\sum_{\kappa=\pm}\int_{-\infty}^\infty dy_0[f_{0,y_0,\kappa} - \delta_{\kappa,-}]$$
$$\times \langle\psi_{0,k_{x\alpha}}^\kappa(\mathbf{r}) \parallel \psi_{0,k_{x\alpha}}^\kappa(\mathbf{r})\rangle, \tag{8}$$

where $f_{n,y_0,\kappa}$ is the Fermi function, the two-component column spinor wave function $\left|\psi_{0,k_{x\alpha}}^\kappa(\mathbf{r})\right\rangle$ is given by Eq. (5); the factor 2 accounts for spin degeneracy. In Eqs. (7),(8) $\kappa = \pm$ is understood as the pseudospin quantum number[16]; e.g., for $y_0 > 0$ only at $(L_y/2 - y_0)/\ell_0 \gg 1$ it

can be well approximated as the valley index. A strong splitting between the electron, $\kappa = +$, and the hole, $\kappa = -$, branches of the $n = 0$ LL[2,6,15], due to hybridization of the valley states take place nearby the armchair edge, at $|L_y/2 - y_0| \leq \ell_0$. The eigenvalues of the $n = 0$ LL for $\kappa = +(-)$ increase (decrease) with increasing y_0. However, for the $n \geq 1$ LLs the $\kappa = \pm$ branches at the armchair edge have a small splitting, due to hybridization of the valley states, as their eigenvalues increase with increasing y_0; these branches are attributed to the electron band. Notice, the electron, $(n = 0, \kappa = +)$, LL stems from the conduction band and the hole, $(n = 0, \kappa = -)$, LL arises from the valence band.

We now consider the situations depicted in Fig. 1 for a wide symmetric armchair graphene ribbon $L_y > 2y_r \gg \Delta y \gg \ell_0$. For definiteness the smooth lateral potential is assumed as follows

$$V(y) = (V_0/2)\Big[2 + \Phi((y-y_r)/\Delta y) + \Phi((y+y_r)/\Delta y)\Big], \tag{9}$$

where $\Phi(x)$ is the probability integral. In Fig. 1 we have $L_y = 18\Delta y$, $V_0 = \hbar v_F/\sqrt{2}\ell_0$, $y_r = 5\Delta y$, and $\Delta y = 10\ell_0$. When the Fermi level E_F is between the bottoms of the $n = 0$ and $n = 1$ LLs, at $y_0 = 0$, and the condition $V_0 \gg 2k_BT$ holds, the occupation of the $n \geq 1$ LLs is negligible; the same holds for the $n = 0$ LL in the regions of y_0 that are well above E_F, see Fig. 1. In addition to the smoothness of the potential Eq.(9), we assume armchair edges of the graphene sheet at $y = \pm L_y/2$, which cause the bending of the LLs,[2,6,15] and $L_y/2 - y_r \geq \Delta y$. For conditions of Fig. 1 and qualitatively similar, the dc magnetotransport measurements will manifest the $\nu = 2$ QHE.

Further, for conditions qualitatively similar with those of Fig. 1, in agreement with speculations of Ref.[16] we will show that a weak periodic potential $V_s(x)$ can have a strong effect on two fundamental EMPs leading to manifestation of the resonance effects. First, for convenience of a reader, we will present expressions for the local Hall conductivity, obtained in Ref.[16], that are pertinent to $V_s(x) \to 0$.

1. Effect of a smooth potential, an armchair edge and a weak periodic potential on local Hall conductivity in the $\nu = 2$ QHE regime

Now, for different regions of the graphene channel we will present expressions as for, obtained in Ref.[16], the unperturbed local Hall conductivity, $\sigma_{yx}^{(0)}(y)$, so for the main contribution induced by a finite $V_s(x)$, $\sigma_{yx}^{(1)}(x,y) \propto V_s$. The superscript in $\sigma_{yx}^{(1)}(x,y)$ indicates that it is of the first order over V_s. Correspondingly, this contribution in Eq. (8) stems from the first order contributions to the wave function Eq. (5); to calculate $\sigma_{yx}^{(1)}(x,y)$ we will need also assume that $V_s/k_BT \ll 1$. Point out that $\sigma_{yx}^{(0)}(y)$ is given by the right hand side of Eq. (8) if to substi-

tute $\left|\psi_{0,k_{x\alpha}}^{\kappa}(\mathbf{r})\right\rangle$, calculated by taking into account the first order corrections, by the zero order wave function $\left|\psi_{0,k_{x\alpha}}^{(0),\kappa}(\mathbf{r})\right\rangle$.

In case (i), for $y_0 > 0$ and $(y_r^d - y_0)/\ell_0 \gg 1$, from Eqs. (3)-(4), (8)-(9) it follows[16]

$$\sigma_{yx}^{(0)}(y) = \frac{2e^2}{h}\tanh\left(\frac{V(y_r^u)-V(y)}{2k_BT}\right), \quad (10)$$

where $V(y)$ is so smooth on the scale of ℓ_0 that $\ell_0 dV(y_r^u)/dy \ll k_BT$; the factor 4 accounts for spin and pseudospin degeneracy. Introducing the characteristic length $\ell_T = \ell_0(k_BT\ell_0/\hbar v_g^u)$, this condition of smoothness can be rewritten as $\ell_0 \ll \ell_T$, where $v_g^u = \ell_0^2\hbar^{-1}dV(y_r^u)/dy$ is the group velocity at the edge y_r^u. Notice, for conditions of Fig. 1 it follows that $v_g^u/v_F = (\ell_0/\sqrt{2\pi}\Delta y) \ll 1$, due to $\ell_0/\Delta y \ll 1$. Point out, Eq. (10) shows that at $y = y_r^u$ the Hall conductivity changes its sign from the electron type of charge carriers to the hole one.

For $(\ell_T/\Delta y)^2 \ll 1$, Eq. (10) can be rewritten as[16]

$$\sigma_{yx}^{(0)}(y) = \frac{2e^2}{h}\tanh\left(\frac{y_r^u - y}{2\ell_T}\right). \quad (11)$$

From Eq. (11) it follows[16,22]

$$\frac{d\sigma_{yx}^{(0)}(y)}{dy} = -\frac{4e^2}{h}\left[\frac{1}{4\ell_T}\cosh^{-2}\left(\frac{y-y_r^u}{2\ell_T}\right)\right]. \quad (12)$$

Further, for $L_y/2 \geq y \geq L_y/2 - 5\ell_0$ pertinent numerical results[6,7,14,15] for $\nu = 2$ we approximate by the same analitical expression for $[n(y) - p(y)]$ as in Ref. 16. That gives

$$\sigma_{yx}^{(0)}(y) = \frac{2e^2}{h}\int_{-\infty}^{\infty}\frac{dy_0}{\sqrt{\pi}\ell_0}e^{-(y-y_0)^2/\ell_0^2}[f_{0,y_0,-} - 1], \quad (13)$$

where it is used that $E_{0,y_0,-}$ is a sharply decreasing function at $y_0 \approx y_r^d$ such that the Fermi function in Eq. (13) is very fastly growing at $y_0 \approx y_r^d$ on a scale $\ell_d \ll \ell_0$. Here appears a new characteristic scale $\ell_d = k_BT\ell_0^2/\hbar|v_g^d|$ as for a change of y_0 on ℓ_d, at $y_0 \approx y_r^d$, the value of $E_{0,y_0,-}$ will change on k_BT; point out that $|v_g^d| \ll v_F$ is implicit in Fig. 1.

From Eq. (13) it follows[16]

$$d\sigma_{yx}^{(0)}(y)/dy = (2e^2/h\sqrt{\pi}\ell_0)e^{-(y-y_r^d)^2/\ell_0^2}, \quad (14)$$

by changing the derivatives over y to those over y_0 and integrating by parts.

In a similar manner, for case (i) and $y > 0$, we obtain from Eqs. (3)-(5), (8) that $\sigma_{yx}^{(1)}(\mathbf{r}) = \sigma_{yx}^{(1)}(y)\cos(Gx)$, where

$$\sigma_{yx}^{(1)}(y) = -\frac{e^2}{h}\frac{V_s}{k_BT}\left[\cosh^{-2}\left(\frac{y-y_r^u}{2\ell_T}\right)\right.$$
$$\left. +\frac{2k_BT\ell_0}{\sqrt{\pi}\hbar|v_g^d|}e^{-(y-y_r^d)^2/\ell_0^2}\right], \quad (15)$$

here it is taken into account that $v_g^d < 0$. Due to $k_BT\ell_0/\hbar|v_g^d| \ll 1$, the amplitude of the second term in the square brackets of Eq. (15) is less than of the first one. In addition, Eq. (15) shows that a small parameter $V_s/k_BT \ll 1$ warrants that $|\sigma_{yx}^{(1)}(x,y)| \ll |\sigma_{yx}^{(0)}(y)|$; in particular, at $y \approx y_r^u$.

III. STRONG RENORMALIZATION OF THE EMPS IN GRAPHENE BY A WEAK SUPERLATTICE POTENTIAL

Now we will study effect of the superlattice potential, $V_s(x)$, on the fundamental EMPs for case (i), i.e., for conditions like in Fig. 1; dissipation is neglected. For $V_s(x) \equiv 0$, our fundamental EMPs will coincide with ones obtained in Ref. 16. Similar with Ref. 16, we expect that the charge excitation due to EMPs at the right part of channel will be strongly localized at y_r^u ($\rho^{ru}(t,\mathbf{r})$) and y_r^d ($\rho^{rd}(t,\mathbf{r})$). Then the components of the current density $\mathbf{j}(\omega,\mathbf{r})$ in the low-frequency limit $\omega \ll v_F/\ell_0$ are given, cf. with,[16] as

$$\begin{aligned} j_x(\omega,\mathbf{r}) = &-[\sigma_{yx}^{(0)}(y) + \sigma_{yx}^{(1)}(\mathbf{r})]E_y(\omega,\mathbf{r}) \\ &+ v_g^u\rho^{ru}(\omega,\mathbf{r}) + v_g^d\rho^{rd}(\omega,\mathbf{r}), \end{aligned} \quad (16)$$

$$j_y(\omega,\mathbf{r}) = [\sigma_{yx}^{(0)}(y) + \sigma_{yx}^{(1)}(\mathbf{r})]E_x(\omega,\mathbf{r}), \quad (17)$$

where we have suppressed the factor $\exp(-i\omega t)$ common to all terms in Eqs. (16) and (17). From Eqs. (16)-(17), Poisson's equation, the linearized continuity equation and using that for EMPs $\mathbf{E}(\omega,\mathbf{r}) = -\nabla\varphi(\omega,\mathbf{r})$), we obtain

$$\begin{aligned} &-i\omega(\rho^{ru}(\omega,\mathbf{r}) + \rho^{rd}(\omega,\mathbf{r})) + [v_g^u\partial_x\rho^{ru}(\omega,\mathbf{r}) \\ &+v_g^d\partial_x\rho^{rd}(\omega,\mathbf{r})] + [\partial_x\sigma_{yx}^{(1)}(\mathbf{r})]\partial_y\varphi(\omega,\mathbf{r}) \\ &-[\partial_y\sigma_{yx}^{(0)}(y) + \partial_y\sigma_{yx}^{(1)}(\mathbf{r})]\partial_x\varphi(\omega,\mathbf{r}) = 0, \end{aligned} \quad (18)$$

where $\partial_x = \partial/\partial x$. Point out, in Eq. (18) the coefficients are invariant for translations along x on any distance integral of the period a_0. Then in Eq. (18) we assume that

$$\rho^{ru}(\omega,\mathbf{r}) = \sum_{\ell=-1}^{1}\rho_\ell^{ru}(\omega,k_x,y)e^{ik_x^{(\ell)}x},$$

$$\rho^{rd}(\omega,\mathbf{r}) = \sum_{\ell=-1}^{1}\rho_\ell^{rd}(\omega,k_x,y)e^{ik_x^{(\ell)}x},$$

$$\varphi(\omega,\mathbf{r}) = \sum_{\ell=-1}^{1}\varphi_\ell(\omega,k_x,y)e^{ik_x^{(\ell)}x}, \quad (19)$$

where $\ell = -1, 0, 1$, $k_x^{(\ell)} = k_x + 2\pi\ell/a_0$, and $k_x \equiv k_x^{(0)}$.

In Eq. (19), for a metallic gate at a distance d from the 2DES (e.g., it can be a heavily doped Si separated from

the graphene sheet by a SiO_2 layer of thickness $d = 300$ nm), is given by

$$\varphi_\ell(\omega, k_x, y) = \frac{2}{\epsilon} \int_{-\infty}^{\infty} dy' R_g(|y - y'|, k_x^{(\ell)}; d)$$
$$\times \left[\rho_\ell^{ru}(\omega, k_x, y') + \rho_\ell^{rd}(\omega, k_x, y') \right], \quad (20)$$

where $R_g(...)$ is given by

$$R_g(|y - y'|, k_x^{(\ell)}; d) = K_0(|k_x^{(\ell)}||y - y'|)$$
$$- K_0(|k_x^{(\ell)}|\sqrt{(y - y')^2 + 4d^2}), \quad (21)$$

where $K_0(x)$ is the modified Bessel function. Without of a metallic gate, $d \to \infty$, the dielectric constant ϵ is spatially homogeneous if not stated otherwise.

Multiplying Eq. (18) by $i \exp(-ik_x x)$ and then integrating over x, $\int_0^{L_x} dx$, we obtain

$$(\omega - k_x v_g^u)\rho_0^{ru}(\omega, k_x, y) + (\omega - k_x v_g^d)\rho_0^{rd}(\omega, k_x, y)$$
$$-\frac{\pi}{a_0}\sigma_{yx}^{(1)}(y)\left[\partial_y \varphi_{-1}(\omega, k_x, y) - \partial_y \varphi_1(\omega, k_x, y)\right]$$
$$+[\partial_y \sigma_{yx}^{(0)}(y)]k_x \varphi_0(\omega, k_x, y) + \frac{1}{2}[\partial_y \sigma_{yx}^{(1)}(y)]$$
$$\times \left[k_x^{(-1)}\varphi_{-1}(\omega, k_x, y) + k_x^{(1)}\varphi_1(\omega, k_x, y) \right] = 0. \quad (22)$$

Further, multiplying Eq. (18) by $i \exp(-ik_x^{(-1)}x)$ and then integrating over x, $\int_0^{L_x} dx$, we obtain

$$(\omega - k_x^{(-1)} v_g^u)\rho_{-1}^{ru}(\omega, k_x, y) + (\omega - k_x^{(-1)} v_g^d)\rho_{-1}^{rd}(\omega, k_x, y)$$
$$+\frac{\pi}{a_0}\sigma_{yx}^{(1)}(y)\partial_y \varphi_0(\omega, k_x, y) + [\partial_y \sigma_{yx}^{(0)}(y)]k_x^{(-1)}\varphi_{-1}(\omega, k_x, y)$$
$$+\frac{1}{2}k_x[\partial_y \sigma_{yx}^{(1)}(y)]\varphi_0(\omega, k_x, y) = 0. \quad (23)$$

In addition, multiplying Eq. (18) by $i \exp(-ik_x^{(1)}x)$ and then integrating over x, $\int_0^{L_x} dx$, we obtain

$$(\omega - k_x^{(1)} v_g^u)\rho_1^{ru}(\omega, k_x, y) + (\omega - k_x^{(1)} v_g^d)\rho_1^{rd}(\omega, k_x, y)$$
$$-\frac{\pi}{a_0}\sigma_{yx}^{(1)}(y)\partial_y \varphi_0(\omega, k_x, y) + [\partial_y \sigma_{yx}^{(0)}(y)]k_x^{(1)}\varphi_1(\omega, k_x, y)$$
$$+\frac{1}{2}k_x[\partial_y \sigma_{yx}^{(1)}(y)]\varphi_0(\omega, k_x, y) = 0. \quad (24)$$

For $y_r^d - y_r^u \gg \ell_T$, from Eqs. (22)-(24) it follows that $\rho_\ell^{ru}(\omega, k_x, y)$ and $\rho_\ell^{rd}(\omega, k_x, y)$ can be well approximated (cf. Ref. 16) as

$$\rho_\ell^{ru}(\omega, k_x, y) = \left[4\ell_T \cosh^2\left(\frac{y - y_r^u}{2\ell_T}\right) \right]^{-1} \rho_\ell^{ru}(\omega, k_x),$$
$$\rho_\ell^{rd}(\omega, k_x, y) = (1/\sqrt{\pi}\ell_0)e^{-(y-y_r^d)^2/\ell_0^2} \rho_\ell^{rd}(\omega, k_x). (25)$$

In addition, we can neglect by overlap between $\rho^{ru}(\omega, k_x, y)$ and $\rho^{rd}(\omega, k_x, y)$ in Eqs. (22)-(24). Then, by integration of Eqs. (22)-(24) over y within separate regions around y_r^u and y_r^d, we obtain by straightforward calculations six coupled linear homogeneous equations for

six unknown functions: $\rho_\ell^{ru}(\omega, k_x)$ and $\rho_\ell^{rd}(\omega, k_x)$, where $\ell = -1, 0, 1$. They read, with $y_r^{du} \equiv y_r^d - y_r^u > 0$,

$$[\omega - \omega_{+,0}^{(i)}(k_x; d)]\rho_0^{ru}(\omega, k_x) - 2c_h k_x R_g(y_r^{du}, k_x; d)$$
$$\times \rho_0^{rd}(\omega, k_x) + c_h k_x \left(\frac{V_s}{k_B T}\ell_T \right) \left[R_g'(y_r^{du}, k_x^{(-1)}; d) \right.$$
$$\times \rho_{-1}^{rd}(\omega, k_x) + R_g'(y_r^{du}, k_x^{(1)}; d)\rho_1^{rd}(\omega, k_x) \Big] = 0, \quad (26)$$

$$[\omega - \omega_{-,0}^{(i)}(k_x; d)]\rho_0^{rd}(\omega, k_x) + c_h k_x R_g(y_r^{du}, k_x; d)$$
$$\times \rho_0^{ru}(\omega, k_x) - c_h k_x \left(\frac{V_s}{k_B T}\ell_T \frac{v_g^u}{2|v_g^d|} \right) \left[R_g'(y_r^{du}, k_x^{(-1)}; d) \right.$$
$$\times \rho_{-1}^{ru}(\omega, k_x) + R_g'(y_r^{du}, k_x^{(1)}; d)\rho_1^{ru}(\omega, k_x) \Big] = 0, \quad (27)$$

$$[\omega - \omega_{+,0}^{(i)}(k_x^{(-1)}; d)]\rho_{-1}^{ru}(\omega, k_x) - 2c_h k_x^{(-1)}$$
$$\times R_g(y_r^{du}, k_x^{(-1)}; d)\rho_{-1}^{rd}(\omega, k_x) + c_h k_x^{(-1)} \left(\frac{V_s}{k_B T}\ell_T \right)$$
$$\times R_g'(y_r^{du}, k_x; d)\rho_0^{rd}(\omega, k_x) = 0, \quad (28)$$

$$[\omega - \omega_{-,0}^{(i)}(k_x^{(-1)}; d)]\rho_{-1}^{rd}(\omega, k_x) + c_h k_x^{(-1)}$$
$$\times R_g(y_r^{du}, k_x^{(-1)}; d)\rho_{-1}^{ru}(\omega, k_x) - c_h k_x^{(-1)} \left(\frac{V_s}{k_B T} \right.$$
$$\times \ell_T \frac{v_g^u}{2|v_g^d|} \Big) R_g'(y_r^{du}, k_x; d)\rho_0^{ru}(\omega, k_x) = 0, \quad (29)$$

$$[\omega - \omega_{+,0}^{(i)}(k_x^{(1)}; d)]\rho_1^{ru}(\omega, k_x) - 2c_h k_x^{(1)}$$
$$\times R_g(y_r^{du}, k_x^{(1)}; d)\rho_1^{rd}(\omega, k_x) + c_h k_x^{(1)} \left(\frac{V_s}{k_B T}\ell_T \right)$$
$$\times R_g'(y_r^{du}, k_x; d)\rho_0^{rd}(\omega, k_x) = 0, \quad (30)$$

$$[\omega - \omega_{-,0}^{(i)}(k_x^{(1)}; d)]\rho_1^{rd}(\omega, k_x) + c_h k_x^{(1)}$$
$$\times R_g(y_r^{du}, k_x^{(1)}; d)\rho_1^{ru}(\omega, k_x) - c_h k_x^{(1)} \left(\frac{V_s}{k_B T} \right.$$
$$\times \ell_T \frac{v_g^u}{2|v_g^d|} \Big) R_g'(y_r^{du}, k_x; d)\rho_0^{ru}(\omega, k_x) = 0, \quad (31)$$

where, by using the same notations as in Ref. 16, we have $c_h = 4e^2/h\epsilon$,

$$\omega_{+,0}^{(i)}(k_x, d) = k_x v_g^u + 2c_h k_x a_p(k_x; d), \quad (32)$$

$$\omega_{-,0}^{(i)}(k_x, d) = -k_x |v_g^d| - c_h k_x a_m(k_x; d), \quad (33)$$

with the matrix elements

$$a_p(k_x; d) = \frac{1}{16} \int_{-\infty}^{\infty} \int_{-\infty}^{\infty} \frac{dx dt R_g(\ell_T|x - t|, k_x; d)}{\cosh^2(x/2)\cosh^2(t/2)}, \quad (34)$$
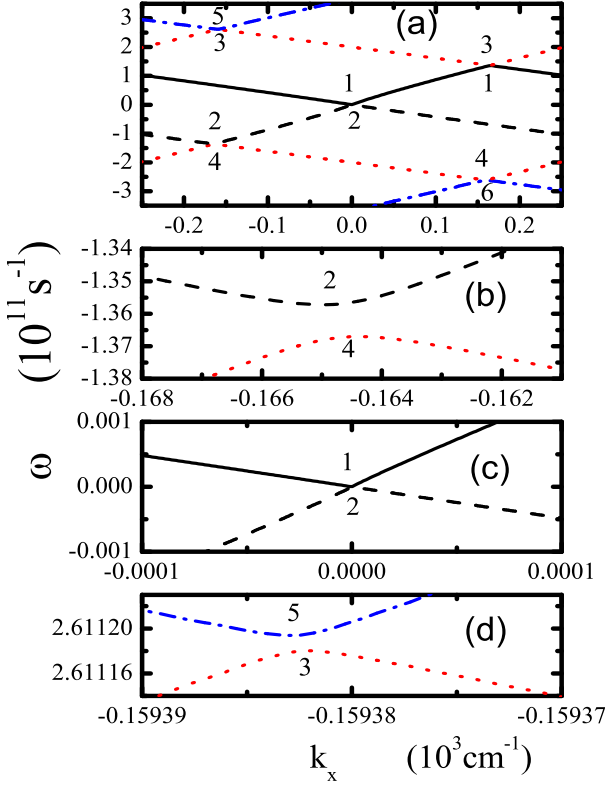
Figure 2: (Color online) The dispersion relations $\omega(k_x, d \to \infty)$, without the gate, of six EMPs calculated from Eqs. (26)-(31) for $2\pi/a_0 = 500\,\text{cm}^{-1}$, $V_s/k_B T = 0.3$, $y_r^{du} = 10\ell_0$, $\Delta y = 10\ell_0$, $B = 9\text{T}$, $T = 77\text{K}$, $\ell_T/\ell_0 = 2$, $v_g^u = 4 \times 10^6$ cm/s, $v_g^d = -3 \times 10^7$ cm/s, $\epsilon = 2$. Panel (a) presents the dispersion relations within the first Brillouin zone, $\pi/a_0 > k_x \geq -\pi/a_0$, by the curves 1 (solid), 2 (dashed), 3 and 4 (dotted), 5 and 6 (dash-dotted). Panel (b) presents a zoom of the anticrossing for the branches 2 and 4, at $k_x \approx -165\,\text{cm}^{-1}$ and $\omega \approx -1.36 \times 10^{11}\,\text{s}^{-1}$, with the gap $\approx 0.98 \times 10^9\,\text{s}^{-1}$; here the EMPs 2 and 4 have a zero value of group velocity for pertinent k_x. Panel (c) presents a zoom of the branches 1 and 2 at $k_x \approx 0$ and $\omega \approx 0$; here a finite gap is absent. Panel (d) presents a zoom of the anticrossing for the branches 3 and 5.
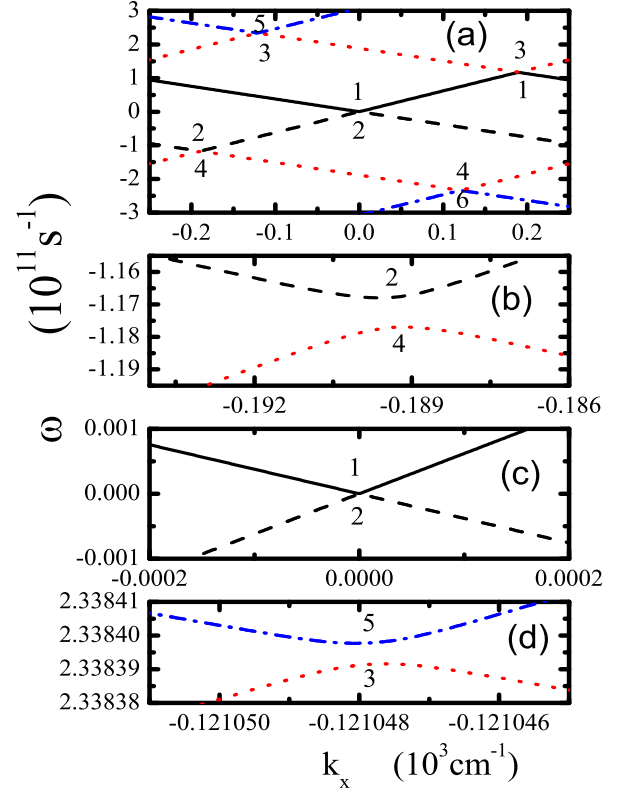
Figure 3: (Color online) The dispersion relations $\omega(k_x, d = 3000\text{nm})$ of six EMPs calculated from Eqs. (26)-(31) for $2\pi/a_0 = 500\,\text{cm}^{-1}$ and other parameters of Fig. 2 except $d = 3000\text{nm}$. Panel (a) presents the dispersion relations within the first Brillouin zone by the curves 1 (solid), 2 (dashed), 3 and 4 (dotted), 5 and 6 (dash-dotted). Panel (b) presents a zoom of the anticrossing for the branches 2 and 4, at $k_x \approx -189\,\text{cm}^{-1}$ and $\omega \approx -1.17 \times 10^{11}\,\text{s}^{-1}$, with the gap $\approx 0.90 \times 10^9\,\text{s}^{-1}$. Panel (c) presents a zoom of the branches 1 and 2 at $k_x \approx 0$ and $\omega \approx 0$. Panel (d) presents a zoom of the anticrossing for the branches 3 and 5.

$$a_m(k_x; d) = \frac{1}{\pi} \int_{-\infty}^{\infty} \int_{-\infty}^{\infty} \frac{dxdt}{e^{x^2+t^2}} R_g(\ell_0|x-t|, k_x; d). \quad (35)$$

Point out, if the graphene is located between two dielectric media with dielectric constants: ϵ_1 for the halfspace below of the graphene, and ϵ_2 for the dielectric layer between the graphene and a metallic gate, - then in all above expressions $\epsilon = (\epsilon_1 + \epsilon_2)/2$.

In addition, in Eqs. (26)-(31)

$$R_g'(y_r^d - y_r^u, k_x; d) = |k_x| \left[K_1(|k_x|y_r^{du}) \right.$$
$$\left. - \frac{y_r^{du}}{\sqrt{(y_r^{du})^2 + 4d^2}} K_1(|k_x|\sqrt{(y_r^{du})^2 + 4d^2}) \right]. \quad (36)$$

Notice that in the long-wavelength limit, $k_x \ell_T \ll 1$, and for large d, such that the effect of gate, $\propto \exp(-2|k_x|d) \ll 1$, can be neglected, from Eqs. (21), (32)-(36) we obtain that: $R_g(|y-y'|, k_x; d) \approx \ln(2/|k_x(y-y')|) - \gamma$, where γ

is the Euler constant, $a_p(k_x; d) \approx [\ln(1/|k_x|\ell_T) - 0.145]$, $a_m(k_x; d) \approx [\ln(1/|k_x|\ell_0) + 3/4]$, and $R_g'(y_r^{du}, k_x; d) \approx 1/y_r^{du}$.

For $\nu = 2$ and case (i), in Fig. 2 we plot the dispersion relations $\omega(k_x, d \to \infty)$ of the EMPs calculated from Eqs. (26)-(31) for $2\pi/a_0 = 500\,\text{cm}^{-1}$, $V_s/k_B T = 0.3$, $y_r^{du} = \Delta y = 10\ell_0$, $B = 9\text{T}$, $T = 77\text{K}$, $\ell_T/\ell_0 = 2$, $v_g^u = 4 \times 10^6$ cm/s, $v_g^d = -3 \times 10^7$ cm/s, $\epsilon = 2$, and $\ell_0 \approx 8.5$ nm. Fig. 2(a) presents the dispersion relations of these EMPs within the first Brillouin zone by the curves 1-6. Notice, Fig. 2(a) shows that the branches 3 and 4 have $\omega \approx \pm 2.0 \times 10^{11}\,\text{s}^{-1}$ at $k_x \approx 0$. Fig. 2(b) presents a zoom of the anticrossing for the branches 2 and 4, at $k_x \approx -165\,\text{cm}^{-1}$ and $\omega \approx -1.36 \times 10^{11}\,\text{s}^{-1}$, with the gap $\approx 0.98 \times 10^9\,\text{s}^{-1}$: here the EMPs 2 and 4 have a zero value of group velocity for pertinent k_x. A panel for the anticrossing of the branches 1 and 3 it follows from the Fig. 2(b) by changing k_x on $-k_x$ and ω on $-\omega$. Fig. 2(c) presents a zoom of the branches 1 and 2 at $k_x \approx 0$ and $\omega \approx 0$; here a finite gap is absent. Panel (d) presents a zoom of the anticrossing for the branches 3 and 5 at
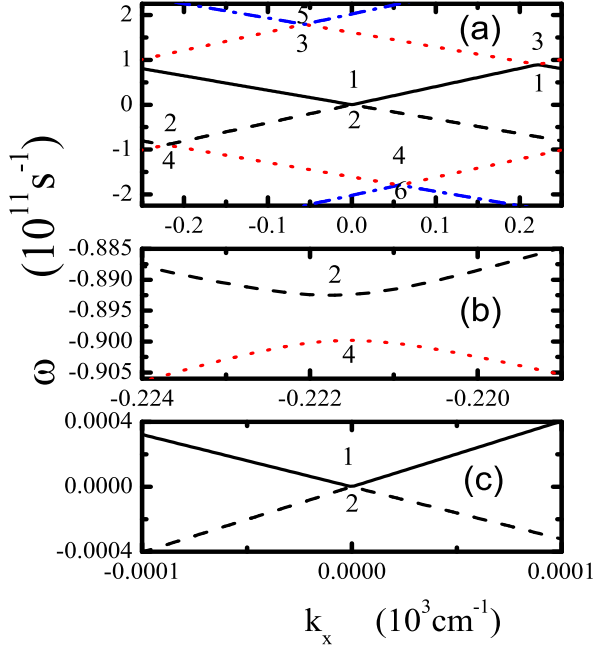
Figure 4: (Color online) The dispersion relations $\omega(k_x, d = 300\text{nm})$ of six EMPs calculated from Eqs. (26)-(31) for $2\pi/a_0 = 500\,\text{cm}^{-1}$ and other parameters of Fig. 2 except $d = 300\text{nm}$. Panel (a) presents the dispersion relations within the first Brillouin zone by the curves 1 (solid), 2 (dashed), 3 and 4 (dotted), 5 and 6 (dash-dotted). Panel (b) presents a zoom of the anticrossing for the branches 2 and 4, at $k_x \approx -222\,\text{cm}^{-1}$ and $\omega \approx -0.90 \times 10^{11}\,\text{s}^{-1}$, with the gap $\approx 0.73 \times 10^9\,\text{s}^{-1}$. Panel (c) presents a zoom of the branches 1 and 2 at $k_x \approx 0$ and $\omega \approx 0$.

$k_x \approx -159.4\,\text{cm}^{-1}$ and $\omega \approx 2.611 \times 10^{11}\,\text{s}^{-1}$, with the gap $\approx 1.37 \times 10^6\,\text{s}^{-1}$.

In Fig. 2 and below, it is used that the exact dispersion relation $\omega(k_x, d)$ of any EMP mode can be presented in the form periodic in the reciprocal space, i.e, $\omega(k_x, d) = \omega(k_x \pm 2\pi/a_0, d)$, and continuous across the borders of the Brillouin zone, $\omega(\pi/a_0 - 0, d) = \omega(\pi/a_0 + 0, d)$. The latter, in particular, does not allow an infinite group velocity for the EMP. Point out that the dispersion curves 1 (solid), 2 (dashed), 3 and 4 (dotted) have correct periodic and continuous form in the reciprocal space, k_x, and both qualitatively and quantavely well describe dispersion of pertinent EMP modes in graphene with the superlattice: 1 and 2 are the main fundamental EMPs, 3 and 4 are the first excited fundamental EMPs. However, an approximate dispersion curves 5 and 6 (dash-dotted) qualitatively correctly represent pertinent exact dependencies only nearby the anticrossings of 5 with 3 and of 6 with 4. So the curves 5 and 6 are shown only within a small part of the first Brillouin zone in Fig. 2(a). In addition, as the second order contributions over the periodic potential are neglected (as well as an additional contributions in Eqs. (19) with the $\ell = \pm 2$) the Fig. 2(d) gives only rough approximation for this anticrossing and, in particular, for its gap.

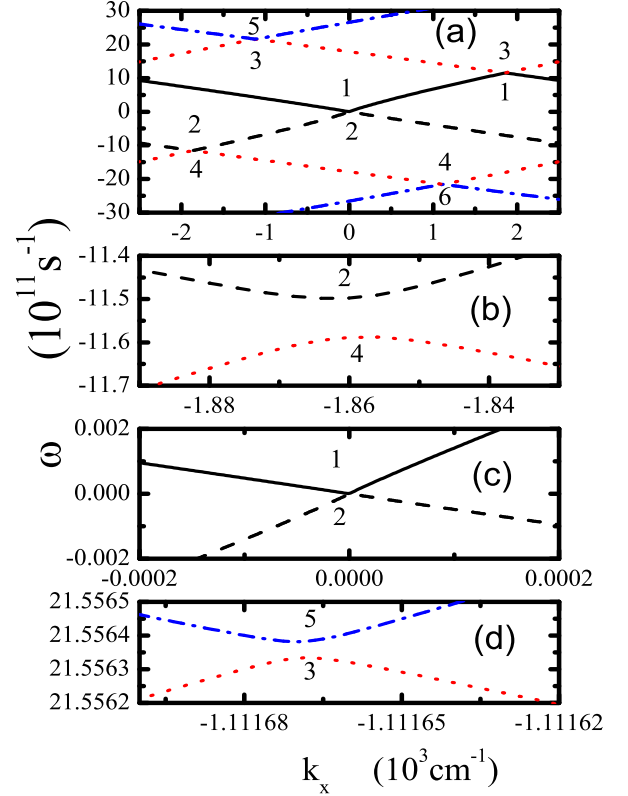In Fig. 3 we plot the dispersion relations $\omega(k_x, d = $

Figure 5: (Color online) The dispersion relations $\omega(k_x, d \to \infty)$, without the gate, of six EMPs calculated from Eqs. (26)-(31) for $2\pi/a_0 = 5000\,\text{cm}^{-1}$, the rest of parameters are the same as in Fig. 2. Panel (a) presents the dispersion relations within the first Brillouin zone, $\pi/a_0 > k_x \geq -\pi/a_0$, by the curves 1 (solid), 2 (dashed), 3 and 4 (dotted), 5 and 6 (dash-dotted). Panel (b) presents a zoom of the anticrossing for the branches 2 and 4, at $k_x \approx -1860\,\text{cm}^{-1}$ and $\omega \approx -1.15 \times 10^{12}\,\text{s}^{-1}$, with the gap $\approx 9.0 \times 10^9\,\text{s}^{-1}$. Panel (c) presents a zoom of the branches 1 and 2 at $k_x \approx 0$ and $\omega \approx 0$; here a finite gap is absent. Panel (d) presents a zoom of the anticrossing for the branches 3 and 5.

3000nm) of the EMPs calculated from Eqs. (26)-(31) for $d = 3000 nm$, the rest of parameters are the same as in Fig. 2. Fig. 3(a) shows that the branches 3 and 4 have $\omega \approx \pm 1.9 \times 10^{11}\,\text{s}^{-1}$ at $k_x \approx 0$. Fig. 3(b) presents a zoom of the anticrossing for the branches 2 and 4, at $k_x \approx -189\,\text{cm}^{-1}$ and $\omega \approx -1.17 \times 10^{11}\,\text{s}^{-1}$, with the gap $\approx 0.90 \times 10^9\,\text{s}^{-1}$: here the EMPs 2 and 4 have a zero value of group velocity for pertinent k_x. A panel for the anticrossing of the branches 1 and 3 it follows from the Fig. 3(b) by changing k_x on $-k_x$ and ω on $-\omega$. Fig. 3(c) presents a zoom of the branches 1 and 2 at $k_x \approx 0$ and $\omega \approx 0$; here a finite gap is absent. Fig. 3(d) presents a zoom of the anticrossing for the branches 3 and 5 at $k_x \approx -121\,\text{cm}^{-1}$ and $\omega \approx 2.34 \times 10^{11}\,\text{s}^{-1}$, with the gap $\sim 5 \times 10^5\,\text{s}^{-1}$.

In Fig. 4 we plot the dispersion relations $\omega(k_x, d = 300\text{nm})$ of the EMPs calculated from Eqs. (26)-(31) for $d = 300 nm$, the rest of parameters are the same as in Fig. 2. Fig. 4(a) shows that the branches 3 and 4 have $\omega \approx \pm 1.6 \times 10^{11}\,\text{s}^{-1}$ at $k_x \approx 0$. Fig. 4(b) presents a
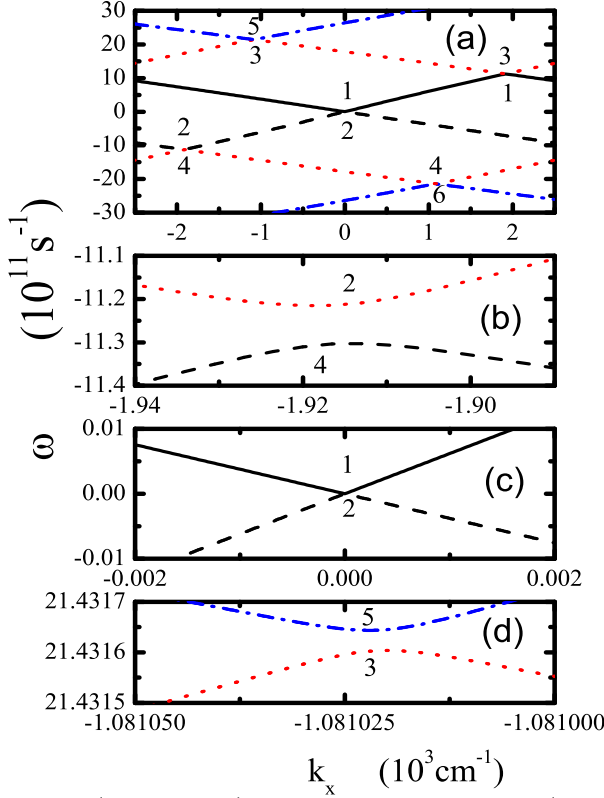
Figure 6: (Color online) The dispersion relations $\omega(k_x, d = 3000\text{nm})$ of six EMPs calculated from Eqs. (26)-(31) for the gate at $d = 3000\text{nm}$; as $2\pi/a_0 = 5000\,\text{cm}^{-1}$ so the other parameters are the same as in Fig. 5. Panel (a) presents the dispersion relations within the first Brillouin zone. Panel (b) presents a zoom of the anticrossing for the branches 2 and 4, at $k_x \approx -1920\,\text{cm}^{-1}$ and $\omega \approx -1.13 \times 10^{12}\,\text{s}^{-1}$, with the gap with the gap $\approx 8.8 \times 10^9\,\text{s}^{-1}$. Panel (c) presents a zoom of the branches 1 and 2 at $k_x \approx 0$ and $\omega \approx 0$; here a finite gap is absent. Panel (d) presents a zoom of the anticrossing for the branches 3 and 5.
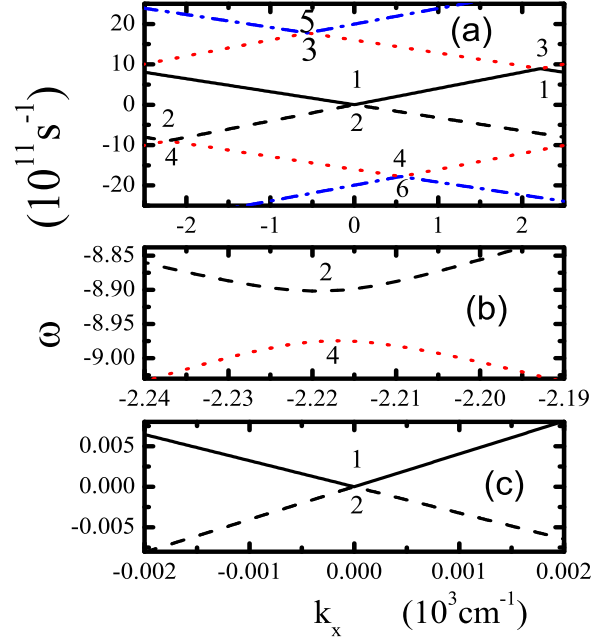

Figure 7: (Color online) The dispersion relations $\omega(k_x, d = 300\text{nm})$ of six EMPs calculated from Eqs. (26)-(31) for $2\pi/a_0 = 5000\,\text{cm}^{-1}$ and other parameters of Fig. 5 except $d = 300\text{nm}$. Panel (a) presents the dispersion relations within the first Brillouin zone. Panel (b) presents a zoom of the anticrossing for the branches 2 and 4, at $k_x \approx -2220\,\text{cm}^{-1}$ and $\omega \approx -8.95 \times 10^{11}\,\text{s}^{-1}$, with the gap $\approx 7.3 \times 10^9\,\text{s}^{-1}$. Panel (c) presents a zoom of the branches 1 and 2 at $k_x \approx 0$ and $\omega \approx 0$; here a finite gap is absent.

zoom of the anticrossing for the branches 2 and 4, at $k_x \approx -222\,\text{cm}^{-1}$ and $\omega \approx -0.90 \times 10^{11}\,\text{s}^{-1}$, with the gap $\approx 7.3 \times 10^8\,\text{s}^{-1}$: here the EMPs 2 and 4 have a zero value of group velocity for pertinent k_x. A panel for the anticrossing of the branches 1 and 3 it follows from the Fig. 4(b) by changing k_x on $-k_x$ and ω on $-\omega$. Fig. 4(c) presents a zoom of the branches 1 and 2 at $k_x \approx 0$ and $\omega \approx 0$; here a finite gap is absent. The anticrossing for the branches 3 and 5 holds at $k_x \approx -56.7\,\text{cm}^{-1}$ and $\omega \approx 1.79 \times 10^{11}\,\text{s}^{-1}$.

In Fig. 5 we plot the dispersion relations $\omega(k_x, d \to \infty)$ of the EMPs calculated from Eqs. (26)-(31) for $2\pi/a_0 = 5000\,\text{cm}^{-1}$ by the curves 1-6. Fig. 5(a) presents the dispersion relations of these EMPs within the first Brillouin zone. Notice, Fig. 5(a) shows that the branches 3 and 4 have $\omega \approx \pm 1.787 \times 10^{12}\,\text{s}^{-1}$ at $k_x \approx 0$. Fig. 5(b) presents a zoom of the anticrossing for the branches 2 and 4, at $k_x \approx -1860\,\text{cm}^{-1}$ and $\omega \approx -1.15 \times 10^{12}\,\text{s}^{-1}$, with the gap $\approx 9.0 \times 10^9\,\text{s}^{-1}$: here the EMPs 2 and 4 have a zero value of group velocity for pertinent k_x. A panel for the anticrossing of the branches 1 and 3 it follows from the

Fig. 5(b) by changing k_x on $-k_x$ and ω on $-\omega$. Fig. 5(c) presents a zoom of the branches 1 and 2 at $k_x \approx 0$ and $\omega \approx 0$; here a finite gap is absent. Panel (d) presents a zoom of the anticrossing for the branches 3 and 5 at $k_x \approx -1112\,\text{cm}^{-1}$ and $\omega \approx 2.16 \times 10^{12}\,\text{s}^{-1}$, with the gap $\sim 5 \times 10^6\,\text{s}^{-1}$.

In Fig. 6 we plot the dispersion relations $\omega(k_x, d = 3000\text{nm})$ of the EMPs calculated from Eqs. (26)-(31) for $2\pi/a_0 = 5000\,\text{cm}^{-1}$. Fig. 6(a) presents the dispersion relations of these EMPs within the first Brillouin zone by the curves 1-6. Notice, Fig. 6(a) shows that the branches 3 and 4 have $\omega \approx \pm 1.783 \times 10^{12}\,\text{s}^{-1}$ at $k_x \approx 0$. Fig. 6(b) presents a zoom of the anticrossing for the branches 2 and 4, at $k_x \approx -1920\,\text{cm}^{-1}$ and $\omega \approx -1.13 \times 10^{12}\,\text{s}^{-1}$, with the gap $\approx 8.8 \times 10^9\,\text{s}^{-1}$: here the EMPs 2 and 4 have a zero value of group velocity for pertinent k_x. A panel for the anticrossing of the branches 1 and 3 it follows from the Fig. 6(b) by changing k_x on $-k_x$ and ω on $-\omega$. Fig. 6(c) presents a zoom of the branches 1 and 2 at $k_x \approx 0$ and $\omega \approx 0$; here a finite gap is absent. Fig. 6(d) presents a zoom of the anticrossing for the branches 3 and 5 at $k_x \approx -1081\,\text{cm}^{-1}$ and $\omega \approx 2.143 \times 10^{12}\,\text{s}^{-1}$, with the gap $\sim 3.7 \times 10^6\,\text{s}^{-1}$.

In Fig. 7 we plot the dispersion relations $\omega(k_x, d = 300\text{nm})$ of the EMPs calculated from Eqs. (26)-(31) for $d = 300\text{nm}$, the rest of parameters are the same as in Fig. 5. Fig. 7(a) shows that the branches 3 and 4 have
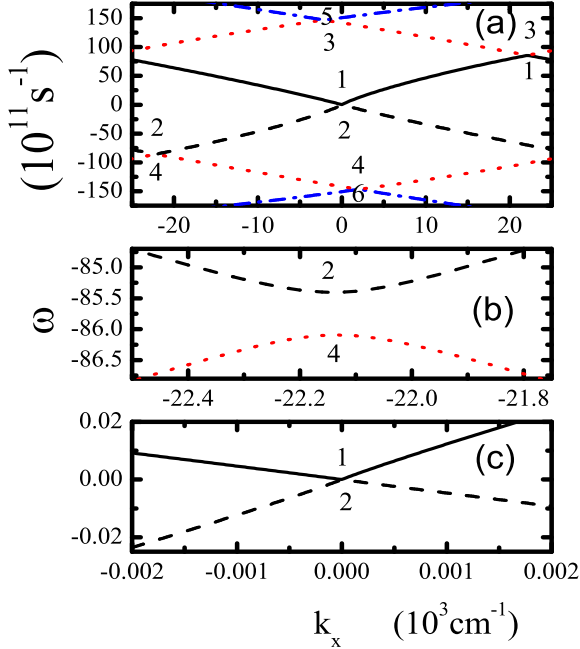
Figure 8: (Color online) The dispersion relations $\omega(k_x, d \to \infty)$, without the gate, of six EMPs calculated from Eqs. (26)-(31) for $2\pi/a_0 = 50000\,\mathrm{cm}^{-1}$, the rest of parameters are the same as in Fig. 2. Panel (a) presents the dispersion relations within the first Brillouin zone, $\pi/a_0 > k_x \geq -\pi/a_0$, by the curves 1 (solid), 2 (dashed), 3 and 4 (dotted), 5 and 6 (dash-dotted). Panel (b) presents a zoom of the anticrossing for the branches 2 and 4, at $k_x \approx -22150\,\mathrm{cm}^{-1}$ and $\omega \approx -8.6 \times 10^{12}\,\mathrm{s}^{-1}$, with the gap $\approx 6.9 \times 10^{10}\,\mathrm{s}^{-1}$. Panel (c) presents a zoom of the branches 1 and 2 at $k_x \approx 0$ and $\omega \approx 0$; a finite gap is absent.
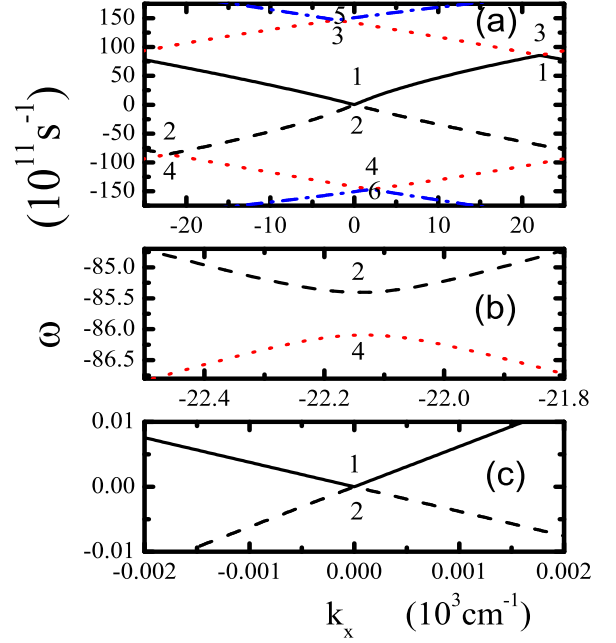

Figure 9: (Color online) The dispersion relations $\omega(k_x, d = 3000\mathrm{nm})$ of the EMPs calculated from Eqs. (26)-(31) for parameters of Fig. 8, except $d = 3000\mathrm{nm}$. Panel (a) presents the dispersion relations within the first Brillouin zone. Panel (b) presents a zoom of the anticrossing for the branches 2 and 4, with the gap $\approx 6.9 \times 10^{10}\,\mathrm{s}^{-1}$. Panel (c) presents a zoom of the branches 1 and 2 at $k_x \approx 0$ and $\omega \approx 0$; a finite gap is absent.

$\omega \approx \pm 1.60 \times 10^{12}\,\mathrm{s}^{-1}$ at $k_x \approx 0$. Fig. 7(b) presents a zoom of the anticrossing for the branches 2 and 4, at $k_x \approx -2220\,\mathrm{cm}^{-1}$ and $\omega \approx -8.95 \times 10^{11}\,\mathrm{s}^{-1}$, with the gap $\approx 7.3 \times 10^9\,\mathrm{s}^{-1}$: here the EMPs 2 and 4 have a zero value of group velocity for pertinent k_x. A panel for the anticrossing of the branches 1 and 3 it follows from the Fig. 7(b) by changing k_x on $-k_x$ and ω on $-\omega$. Fig. 7(c) presents a zoom of the branches 1 and 2 at $k_x \approx 0$ and $\omega \approx 0$; here a finite gap is absent.

In Fig. 8 we plot the dispersion relations $\omega(k_x, d \to \infty)$ of the EMPs calculated from Eqs. (26)-(31) for $2\pi/a_0 = 50000\,\mathrm{cm}^{-1}$. Fig. 8(a) presents the dispersion relations of these EMPs within the first Brillouin zone by the curves 1-6. Notice, Fig. 8(a) shows that the branches 3 and 4 have $\omega \approx \pm 1.42 \times 10^{13}\,\mathrm{s}^{-1}$ at $k_x \approx 0$. Fig. 8(b) presents a zoom of the anticrossing for the branches 2 and 4, at $k_x \approx -22150\,\mathrm{cm}^{-1}$ and $\omega \approx -8.6 \times 10^{12}\,\mathrm{s}^{-1}$, with the gap $\approx 6.9 \times 10^{10}\,\mathrm{s}^{-1}$: here the EMPs 2 and 4 have a zero value of group velocity for pertinent k_x. A panel for the anticrossing of the branches 1 and 3 it follows from the Fig. 5(b) by changing k_x on $-k_x$ and ω on $-\omega$. Fig. 8(c) presents a zoom of the branches 1 and 2 at $k_x \approx 0$ and $\omega \approx 0$; here a finite gap is absent.

In Fig. 9 we plot the dispersion relations $\omega(k_x, d = 3000\mathrm{nm})$ of the EMPs calculated from Eqs. (26)-(31)

for $d = 3000\mathrm{nm}$; in addition, $2\pi/a_0 = 50000\,\mathrm{cm}^{-1}$ and other parameters coincide with those of Fig. 8. Fig. 9(a) presents the dispersion relations of these EMPs within the first Brillouin zone by the curves 1-6. Notice, Fig. 9(a) shows that the branches 3 and 4 have $\omega \approx \pm 1.42 \times 10^{13}\,\mathrm{s}^{-1}$ at $k_x \approx 0$. Fig. 9(b) presents a zoom of the anticrossing for the branches 2 and 4, at $k_x \approx -22150\,\mathrm{cm}^{-1}$ and $\omega \approx -8.6 \times 10^{12}\,\mathrm{s}^{-1}$, with the gap $\approx 6.9 \times 10^{10}\,\mathrm{s}^{-1}$: notice, the parameters of this anticrossing are very close to the ones of similar anticrossing in Fig. 8(b). A panel for the anticrossing of the branches 1 and 3 it follows from the Fig. 9(b) by changing k_x on $-k_x$ and ω on $-\omega$. Fig. 9(c) presents a zoom of the branches 1 and 2 at $k_x \approx 0$ and $\omega \approx 0$; here a finite gap is absent.

In Fig. 10 we plot the dispersion relations $\omega(k_x, d = 300\mathrm{nm})$ of the EMPs calculated from Eqs. (26)-(31) for $d = 300\mathrm{nm}$; in addition, $2\pi/a_0 = 50000\,\mathrm{cm}^{-1}$ and other parameters coincide with those of Fig. 8. Fig. 10(a) presents the dispersion relations of these EMPs within the first Brillouin zone by pertinent curves, 1-6. Notice, Fig. 10(a) shows that the branches 3 and 4 have $\omega \approx \pm 1.41 \times 10^{13}\,\mathrm{s}^{-1}$ at $k_x \approx 0$. Fig. 10(b) presents a zoom of the anticrossing for the branches 2 and 4, at $k_x \approx -22900\,\mathrm{cm}^{-1}$ and $\omega \approx -8.2 \times 10^{12}\,\mathrm{s}^{-1}$, with the gap $\approx 6.7 \times 10^{10}\,\mathrm{s}^{-1}$. Notice, the parameters of this anticrossing are close to the ones in Fig. 8(b), in particular, in Fig. 10(b) the gap is only 3% smaller than in Fig. 8(b).
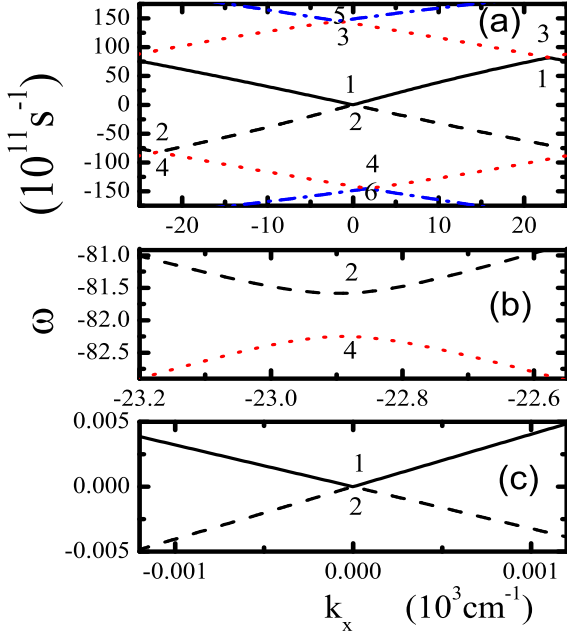
Figure 10: (Color online) The dispersion relations $\omega(k_x, d = 300\text{nm})$ of the EMPs calculated from Eqs. (26)-(31) for parameters of Fig. 8, except $d = 300\text{nm}$. Panel (a) presents the dispersion relations within the first Brillouin zone. Panel (b) presents a zoom of the anticrossing for the branches 2 and 4, at $k_x \approx -22900\,\text{cm}^{-1}$ and $\omega \approx -8.2 \times 10^{12}\,\text{s}^{-1}$, with the gap $\approx 6.7 \times 10^{10}\,\text{s}^{-1}$. Panel (c) presents a zoom of the branches 1 and 2 at $k_x \approx 0$ and $\omega \approx 0$; a finite gap is absent.

A panel for the anticrossing of the branches 1 and 3 it follows from the Fig. 10(b) by changing k_x on $-k_x$ and ω on $-\omega$. Fig. 10(c) presents a zoom of the branches 1 and 2 at $k_x \approx 0$ and $\omega \approx 0$; here a finite gap is absent. Notice, Fig. 10(a) shows that the anticrossing of the curves 3 and 5 takes place at $k_x \approx 1730\,\text{cm}^{-1}$ and $\omega \approx 1.45 \times 10^{13}\,\text{s}^{-1}$.

It is natural to call in Figs. 2-10: the fundamental EMPs 1, 2 as the main fundamental EMPs, and the fundamental EMPs 3, 4 as the first excited fundamental EMPs. Figs. 2-10 show that for case (i), outlined in Fig.1, a strong Bragg coupling is possible due to a weak superlattice along the edge, with the period a_0, if $L_x/a_0 \gg 1$. In particular, for frequencies in the THz range: cf. Figs. 8-10. We expect that for the frequency that corresponds to zero group velocity of pertinent main fundamental EMP branch, or pertinent first excited fundamental EMP branch, and its vicinity the response of the system will have a strong resonance.

IV. CONCLUDING REMARKS

At the edge of a wide armchair graphene ribbon in the $\nu = 2$ QHE regime and with a smooth monotonic electrostatic potential, we investigated the appearance of EMPs that show zero group velocity, for characteristic frequencies, and finite frequency gaps due to effect of

a weak superlattice potential. The superlattice potential from two original fundamental EMPs (present here without superlattice[16]), due to a strong Bragg alike coupling of them, gives correctly within as a whole first Brillouin zone two main fundamental EMPs (branches 1 and 2 on Figs. 2-10) and two first excited fundamental EMPs (branches 3 and 4 on Figs. 2-10). In addition, for the wave vector within the center of the first Brillouin zone, i.e., $k_x \to 0$, only the frequencies of the main fundamental EMPs, 1 and 2, tend to zero as the frequencies, e.g., of the first excited fundamental EMPs, 3 and 4, tend to finite values. As at the frequency that corresponds to zero group velocity of the main fundamental EMPs so at one for the first excited fundamental EMPs the response of the system should have a strong resonance, e.g., in the THz range; see Figs. 8-10.

Next we list and discuss the approximations used. Point out that in Fig. 1 (as well as in Fig. 1 of[16]) it is implicit that $(v_g(k_{x\alpha})/v_F)^2 \ll 1$ for any shown $y_0 = \ell_0^2 k_{x\alpha}$. Then extra Dirac points in the energy spectrum[11–13] due to present smooth, weak superlattices will not appear as here it follows that $\hbar v_F G \gg V_s/2$, which is opposite to the key condition for extra Dirac points.[11,12] Here for the EMPs in the $\nu = 2$ QHE regime dissipation is neglected, which is well justified as here the EMP damping can be related only with inelastic scattering processes within narrow temperature belts, of width $k_B T$, of each edge state that are much weaker than scattering processes due to a static disorder.[16] The latter makes a dominant contribution to the transport scattering time in a 2DES of graphene[1,2,33] for $B = 0$. Needless to say that for a more accurate account of the EMPs studied here, dissipation must be included in the treatment. We have neglected by nonlocal effects that usually have minor effect on fundamental EMPs[23]. We emphasize that our study of the fundamental EMPs for the armchair termination of a graphene channel cannot be directly extended to zigzag termination as some important properties of the wave functions and the energy levels are different than those of the armchair termination, cf.[2,6–8,14]. We relegate the study of EMPs along zigzag edges to a future work.

It is used a simple analytical model of a smooth, lateral confining potential Eq. (9), however, our main results are robust to modifications of its form and parameters if the qualitative conditions of Fig. 1 are realized in a graphene channel in the $\nu = 2$ QHE regime. In Figs. 2-10 it is used that the exact dispersion relation $\omega(k_x, d)$ of any EMP mode can be presented in the form periodic in the reciprocal space, i.e, $\omega(k_x, d) = \omega(k_x \pm 2\pi/a_0, d)$, and continuous across the borders of the Brillouin zone, $\omega(\pi/a_0 - 0, d) = \omega(\pi/a_0 + 0, d)$. The latter, in particular, does not allow an infinite group velocity for the EMP. Point out that the dispersion curves of first four EMP modes, 1 - 4 , have correct periodic and continuous form in the reciprocal space, k_x, and both qualitatively and quantivately well describe dispersion of these EMP modes in graphene with the superlattice. However, an

approximate dispersion curves 5 and 6 (dash-dotted) in Figs. 2-10 qualitatively correctly represent pertinent exact dependencies only nearby the anticrossings of 5 with 3 and of 6 with 4. So the curves 5 and 6 are shown only within a small part of the first Brillouin zone in Figs. 2(a)-10(a). In addition, as the second order contributions over the periodic potential are neglected (as well as an additional contributions in Eqs. (19) with the $\ell = \pm 2$) the Figs. 2(d), 3(d), 5(d), 6(d) give only rough approximation for this anticrossing and, in particular, for its gap.

[1] K. S. Novoselov, A. K. Geim, S. V. Morozov, D. Jiang, Y. Zhang, S. V. Dubonos, I. V. Grigorieva, and A. A. Firsov, Science **306**, 666 (2004); K. S. Novoselov, *Proc. Natl. Acad. Sci. USA* **102**, 10451 (2005); A. K. Geim and K. S. Novoselov, Nature Materials, **6**, 183 (2007).

[2] A. H. Castro Neto, F. Guinea, N. M. R. Peres, K. S. Novoselov, and A. K. Geim, Rev. Mod. Phys. **81**, 109 (2009).

[3] P. R. Wallace, Phys. Rev. **71**, 622 (1947).

[4] O. Klein, Z. Phys. **53**, 157 (1929).

[5] M. I. Katsnelson, K. S. Novoselov, A. K. Geim, Nature Phys. **2**, 620 (2006); J. Milton Pereira Jr., P. Vasilopoulos, and F. M. Peeters, Appl. Phys. Lett. **90**, 132122, (2007).

[6] L. Brey and H. A. Fertig, Phys. Rev. B **73**, 195408 (2006); N. M. R. Peres, F. Guinea, A. H. Castro Neto, *ibid* **73**, 125411 (2006).

[7] D. A. Abanin, P. A. Lee, and L. S. Levitov, Phys. Rev. Lett. **96**, 176803 (2006); Solid State Commun., **143**, 77 (2007).

[8] V. P. Gusynin, V. A. Miransky, S. G. Sharapov, and I. A. Shovkovy, Phys. Rev. B **77**, 205409 (2008).

[9] N. M. R. Peres, A. H. Castro Neto, F. Guinea, Phys. Rev. B **73**, 241403 (2006).

[10] H.-Y. Chen, V. Apalkov, and T. Chakraborty, Phys. Rev. Lett. **98**, 186803 (2007); A. V. Shytov, M. S. Rudner, and L. S. Levitov, *ibid* **101**, 156804 (2008).

[11] C.-H. Park, Y.-W. Son, Li Yang, M. L. Cohen, and S. G. Louie, Phys. Rev. Lett. **103**, 046808 (2009).

[12] L. Brey and H. A. Fertig, Phys. Rev. Lett. **103**, 046809 (2009).

[13] M. Barbier, P. Vasilopoulos, and F. M. Peeters, Phys. Rev. B **81**, 075438 (2010); M. Barbier, F. M. Peeters, P. Vasilopoulos, and J.M. Pereira, *ibid* **77**, 115446 (2008).

[14] V. P. Gusynin, V. A. Miransky, S. G. Sharapov, I. A. Shovkovy, and C. M. Wyenberg, Phys. Rev. B **79**, 115431 (2009).

[15] J.M. Pereira, F. M. Peeters, and P. Vasilopoulos, Phys. Rev. B **75**, 125433 (2007).

[16] O.G. Balev, P. Vasilopoulos, and H. O. Frota, Phys. Rev. B **84**, 245406 (2011).

[17] V.A. Volkov and S.A. Mikhailov, "Electrodynamics of Two-Dimensional Electron Systems in High Magnetic Fields," in Landau Level Spectroscopy, Modern Problems in Condensed Matter Sciences, Ed. by G. Landwehr and E. I. Rashba (North-Holland, Amsterdam, 1991), vol. 27.2, ch.15, p. 855-907; V.A. Volkov and S.A. Mikhailov, Zh. Eksp. Teor. Fiz. **94**, 217 (1988) [Sov. Phys. JETP **67**, 1639 (1988)].

[18] I. L. Aleiner and L. I. Glazman, Phys. Rev. Lett. **72**, 2935 (1994).

[19] B. I. Halperin, Phys. Rev. B **25**, 2185 (1982); X. G. Wen, *ibid* **43**, 11025 (1991); M. Stone, Ann. Phys. (N.Y.) **207**, 38 (1991).

[20] M. Stone, H. W. Wyld, and R. L. Schult, Phys. Rev. B **45**, 14156 (1992); U. Zulicke and A. H. MacDonald, *ibid* **54**, 16813 (1996); S. Giovanazzi, L. Pitaevskii, and S. Stringari, Phys. Rev. Lett. **72**, 3230 (1994).

[21] O. G. Balev and P. Vasilopoulos, Phys. Rev. Lett. **81**, 1481 (1998); O.G. Balev, P. Vasilopoulos, and Nelson Studart, J. Phys.: Condens. Matter **11**, 5143 (1999); O. G. Balev and P. Vasilopoulos, Phys. Rev. B **56**, 13252 (1997).

[22] O. G. Balev and Nelson Studart, Phys. Rev. B **61**, 2703 (2000); Sanderson Silva and O. G. Balev, J. Appl. Phys. **107**, 104310 (2010).

[23] O. G. Balev and P. Vasilopoulos, Phys. Rev. B **59**, 2807 (1999).

[24] R. C. Ashoori, H. L. Stormer, L. N. Pfeiffer, K. W. Baldwin, and K. West, Phys. Rev. B **45**, 3894 (1992).

[25] G. Ernst, R. J. Haug, J. Kuhl, K. von Klitzing, and K. Eberl, Phys. Rev. Lett. **77**, 4245 (1996).

[26] M. N. Khannanov, A. A. Fortunatov, and I. V. Kukushkin, Pis'ma Zh. Eksp. Teor. Fiz. **90**, 740 (2009) [JETP Lett.**90**, 667 (2009)].

[27] O. G. Balev, Nelson Studart, and P. Vasilopoulos, Phys. Rev. B **62**, 15834 (2000).

[28] L.D. Landau and E.M. Lifshitz, *Quantum Mechanics* (Pergamon Press, New York, 1975).

[29] C. W. J. Beenakker and H. van Houten, in *Quantum Transport in Semiconductor Nanostructures*, Solid State Physis Vol. 44 edited by H. Ehrenreich and D. Turnbull (Academic, San Diego, 1991).

[30] D. J. Thouless, Phys. Rev. Lett. **71**, 1879 (1993).

[31] O. G. Balev and P. Vasilopoulos, Phys. Rev. B **54**, 4863 (1996).

[32] Y. Zheng and T. Ando, Phys. Rev. B **65**, 245420 (2002); V. P. Gusynin and S. G. Sharapov, Phys. Rev. Lett. **95**, 146801 (2005).

[33] O. G. Balev, F. T. Vasko, and V. Ryzhii, Phys. Rev. B **79**, 165432 (2009).